Journal of Alloys and Compounds 505 (2010) 224–228

Contents lists available at ScienceDirect

Journal of Alloys and Compounds

journal homepage: www.elsevier.com/locate/jallcom

Characterization of rare-earth doped Lu_2O_3 nanopowders prepared with polymer complex solution synthesis

Radenka Krsmanović [a,*], Željka Antić [a], Barbora Bártová [b], Miroslav D. Dramićanin [a]

[a] Laboratory for Radiation Chemistry and Physics, Vinča Institute of Nuclear Sciences, University of Belgrade, P.O. Box 522, 11001 Belgrade, Serbia
[b] LSME&CIME, École Polytechnique Fédérale de Lausanne, Station 12, CH-1015 Lausanne, Switzerland

ARTICLE INFO

Article history:
Received 4 March 2010
Received in revised form 1 June 2010
Accepted 10 June 2010
Available online 16 June 2010

Keywords:
Phosphors
Oxide materials
Chemical synthesis
Luminescence

ABSTRACT

We explored a synthesis route based on the polymer complex solution method for the production of the rare-earth doped Lu_2O_3 crystalline nanopowders. In this type of synthesis polyethylene glycol is used both as fuel for the combustion reaction, and as nucleation agent for the crystallization process. Synthesized materials were characterized with X-ray diffraction technique, scanning and transmission electron microscopy, EDX technique and photoluminescence spectroscopy with steady state and time domain measurements. X-ray diffraction and electron diffraction analysis showed that presented synthesis procedure yields pure-phase, well crystallized Lu_2O_3 nanopowders with the particles dimensions in the 30–50 nm range, as observed from TEM images. Luminescence properties of Sm^{3+} and Tb^{3+} doped Lu_2O_3 exhibited characteristic red and pseudo-white emissions from these rare-earth ions, with an average emission lifetime of 0.8 and 0.6 ms, respectively.

1. Introduction

Rare-earth luminescent materials have attracted much attention because of their applications in artificial lights, X-ray medical radiography, lamps and display devices and high-power solid-state lasers. Among them, rare-earth (RE) sesquioxides are well-recognized host materials due to good chemical stability, adequate thermal conductivity and high light output. In particular the lutetium oxide has been regarded as a promising host for the detectors of ionizing radiation, such as gamma particles and X-rays. High performance of such detectors is ascribed to the exceptionally high density (~9.42 g/cm^3) of Lu_2O_3 that combined with the high Z number of Lu (71) endows a high stopping power for ionizing radiation [1]. In addition, Lu_2O_3 cubic crystal structure makes the preparation of polycrystalline transparent ceramics possible, starting from the powder [2,3]. Actually, this is of great importance, as the high melting point of this compound, around 2763 K, makes single crystal growth difficult with standard growth methods.

Oxide-based phosphors are traditionally prepared by a solid-state reaction method starting with a mechanical mixing of precursor oxides, followed by ball-milling and calcination. The common problems of this method are poor sintering behavior of the material, nonhomogeneity, imprecise control of cation stoichiometry and high processing temperature [4].

To overcome these problems, wet chemical processes such as hydrothermal synthesis [5], co-precipitation [6–8] and sol–gel [9] have been used as common synthesis methods for rare-earth doped lutetia. However, these chemical methods involve complicated steps, such as precise control of pH and precipitation, in order to obtain the correct stoichiometric compound. On the other hand, combustion synthesis emerged in the last decade as an important synthesis technique for oxide nanoparticles, for being very simple, fast and cost-effective [10,11].

In this study, we used polymer complex solution (PCS) method—a modified combustion route, for the production of Sm and Tb doped lutetia nanoparticles. The utility of this polymeric approach is two folded: (*i*) chelating of cations onto polymer chains providing dopant mixing at atomic level, and (*ii*) development of extremely high viscosity polymeric raisins during the gelation process resulting in a very low cation mobility [12]. The luminescence performance, structure and morphology of synthesized materials were systematically examined and results are reported and discussed herein.

2. Materials and methods

Two samples of Lu_2O_3 metal oxide doped with 3 at.% of Sm^{3+} and Tb^{3+} ions were produced with PCS method. First we prepared water solutions of stoichiometric quantities of RE-nitrates by dissolving appropriate quantities of rare-earth oxides in hot nitric acid. To such obtained solutions polyethylenglycol (PEG), with molecular weight of 200, was added in 1:1 mass ratio to used oxides. After metal-PEG solution formation and continuous stirring at 80 °C for few hours, a metal-PEG solid complex was formed. Subsequently, this complex was combusted at 800 °C in a furnace at atmospheric pressure,

* Corresponding author. Tel.: +381 11 3408 195; fax: +381 11 3408 607.
E-mail address: radenka@vinca.rs (R. Krsmanović).

0925-8388/$ – see front matter © 2010 Elsevier B.V. All rights reserved.
doi:10.1016/j.jallcom.2010.06.033

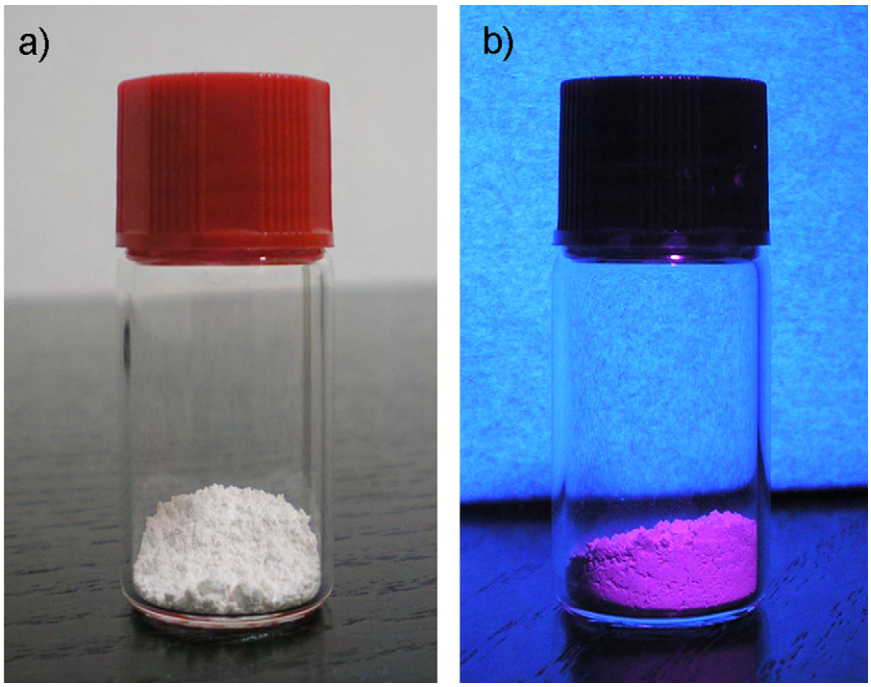

Fig. 1. Photo of Lu_2O_3:Sm^{3+} powder (a) as-synthesized, (b) emitting strong red light under UV excitation.

and kept at the same temperature for 2 h. As a final result, white color of Sm^{3+} doped (see Fig. 1) and pale-sand color Tb^{3+} doped Lu_2O_3 powders were obtained.

X-ray diffraction (XRD) measurements were obtained on Philips PW 1050 instrument, using Ni filtered Cu $K\alpha_{1,2}$ radiation, in a 2θ range from 10° to 120°, counting for 12 s in 0.02° steps. Structure analysis was performed using Koalariet software based on Rietveld full profile refinement method [13].

Microstructure of the calcinated samples was examined with scanning (SEM JEOL JSM 6460LV) and transmission electron microscopy (TEM Philips/FEI CM300). The composition of the powders was checked with EDX (energy dispersive X-ray spectroscopy) measurements done with X-ray microanalysis unit (Oxford Instruments) attached to SEM.

Photoluminescence measurements were performed at room temperature on the Fluorolog-3 Model FL3-221 spectroflurometer system (Horiba Jobin-Yvon), utilizing a 450-W xenon lamp as an excitation source for emission measurements and a xenon-mercury pulsed lamp for lifetime measurements. Time-correlated single-photon counting (TCSPC) method was used to provide luminescence lifetime values from the fluorescence decay curves. TBX-04-D PMT detector was used for both lifetime and steady state acquisitions.

EDX and luminescence experiments were done on pellets prepared from the powders under the load of 5 tones and without any additives.

3. Results and discussion

Lu_2O_3 crystallizes in the cubic bixbyite structure of $Ia\bar{3}$ space group, with lattice constant $a = 1.039$ nm [14]. This structure offers two crystallographically inequivalent sites for Lu^{3+} ions: non-centrosymmetric C_2 and centrosymmetric S_6 (C_{3i}), which can be occupied either by Sm^{3+} or Tb^{3+} dopant ions. Due to their lower symmetry and greater abundance in the structure, lanthanide ions preferably populate the C_2 sites.

Our XRD analyses confirmed that, after calcination at 800 °C for 2 h, powder samples crystallize in a cubic phase of Lu_2O_3 (JCPDS No. 12-0728). Measured XRD pattern for Lu_2O_3:Sm^{3+} sample is given in Fig. 2, together with calculated and difference patterns. The following crystallographic data were obtained from the Rietveld analysis: crystal coherence size of 28(1) nm, unit cell parameter $a = 10.4295(4)$ Å, microstrains $\Delta a/a = 0.318(14)$%.

SEM observations revealed that at micron-level our powders had quite dense morphology (Fig. 3A), different from fluffy and sponge-like appearance typical for powders, produced with standard combustion methods [15–17]. This characteristic can be ascribed to the use of PEG in the synthesis procedure.

Qualitative EDX analysis, performed on SEM, confirmed the presence of RE dopants and the purity of our materials. One spectrum for Lu_2O_3:Sm^{3+}, acquired for 100 s at the accelerating voltage of 25 kV, is presented in Fig. 3B. The chemical homogenity of the samples was checked using EDX mapping technique. The elemental maps of Lu, Sm (Tb) and O (not presented here) showed a uniform density distribution, thus confirming that the activators distribution is homogeneous throughout the material.

TEM observations at nanometer level showed the presence of agglomerates, made up of nanoparticles sized in the range of 30–50 nm (Fig. 4A). High-resolution TEM examinations revealed a

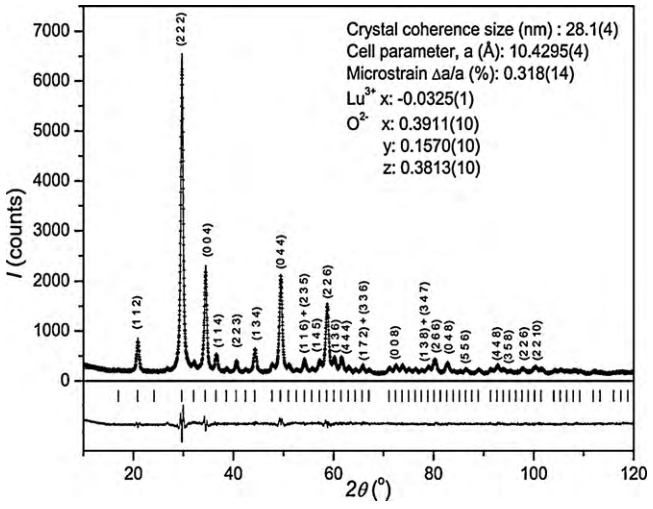

Fig. 2. Observed (crosses), calculated (solid line) and difference XRD patterns of Sm^{3+} doped Lu_2O_3 powder sample; the diffraction peaks are indexed according to JCPDS card No. 12-0728. Crystallographic data obtained from the Rietveld analysis are shown as inset. Thick marks denote the peak positions of Bragg reflections of Lu_2O_3 cubic phase.

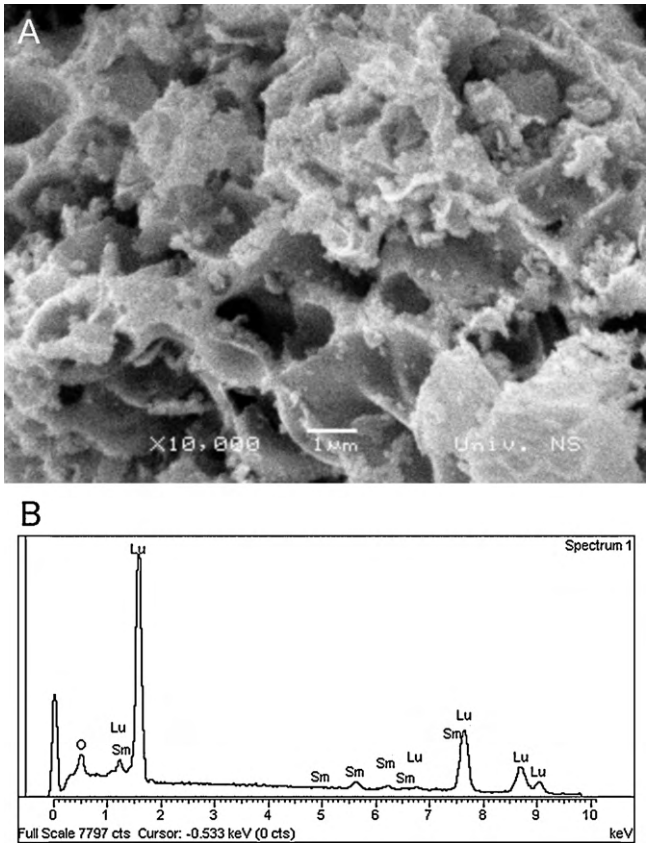

Fig. 3. Typical SEM image (A) and EDX spectrum (B) for Sm^{3+} doped Lu_2O_3 sample.

good crystalline structure of those nanoparticles, without any irregularities or amorphous surface layer (Fig. 4B). The local crystalline structure was investigated by electron diffraction (ED). Experimental ring diffraction pattern is given as an upper inset in Fig. 4A. The same ring ED pattern, with marked Miller indices of Lu_2O_3 and rings intensity as obtained from the simulation on JEMS software [18], is shown bellow in the same figure. The crystalline structure of Lu_2O_3 was built in JEMS software based on the data obtained from XRD measurements.

The results of the photoluminescent investigation are presented in Fig. 5. As we already mentioned, due to the lower symmetry and the greater abundance in the structure it is expected that dopant lanthanide ions preferably substitute Lu^{3+} in C_2 site. For lanthanide ions residing in C_2 site, the f–f transitions are partially allowed by forced electric-dipole due to odd parity terms in the crystal field Hamiltonian. On the other hand, for lanthanide ions situated in the S_6 sites of inversion symmetry, only weak magnetic-dipole induced transitions are possible. Therefore, we presume that observed strong luminescence in Lu_2O_3 samples arises from Sm^{3+} and Tb^{3+} ions situated in non-centrosymmetric C_2 crystallographic positions. The strong crystal field of Lu_2O_3 host results in prominent Stark splitting, and we calculated the position of the barycenters for each observed transition.

Emission spectrum of Sm^{3+} doped sample was recorded at room temperature under the excitation of 406 nm. The reddish-orange light of Sm^{3+} ions consists of three emission bands in the visible region (see Fig. 5a) which have to be assigned to the intra-4f-shell $^4G_{5/2} \rightarrow {}^6H_J$ transitions ($J = 5/2$, 7/2 and 9/2, respectively) of the Sm^{3+} ion [19]. For each transition the correspondent barycenter was calculated and following values were obtained: 574.60, 612.37 and 661.73 nm, respectively. The transition $^4G_{5/2} \rightarrow {}^6H_{5/2}$ (peaks at 570, 577 and 586 nm) has a predominant magnetic-dipole character ($\Delta J = 0$) while $^4G_{5/2} \rightarrow {}^6H_{9/2}$ (650, 656, 662.5, 669.5 and 676.5 nm) transition is magnetic-dipole forbidden and electric-dipole allowed. The red emission peak of the highest intensity corresponds to $^4G_{5/2} \rightarrow {}^6H_{7/2}$ transition (597.5, 608, 618.5 and 625 nm) and is positioned at 608 nm wavelength. The crystal field splitting of Sm^{3+} ion has a maximum number of $(J + 1/2)$-manifolds for the $^4G_{5/2} \rightarrow {}^6H_J$ transitions (3 for $J = 5/2$, 4 for 7/2 and 5 for 9/2) that confirmed our hypothesis of C_2-site occupancy.

Emission spectrum of Tb^{3+} doped sample was recorded at room temperature under the excitation of 350 nm (Fig. 5b). In this case the characteristic emission of Tb^{3+} was distributed into four groups, corresponding to the following f-f transitions $^5D_4 \rightarrow {}^7F_6$ (483.5, 488.5, 492, 497.5, 502.5 nm), $^5D_4 \rightarrow {}^7F_5$ (542, 548, 550.5, 552, 554 nm), $^5D_4 \rightarrow {}^7F_4$ (578.5, 580, 583, 585, 588.5, 590.5, 593, 598, 595.5, 600 nm), $^5D_4 \rightarrow {}^7F_3$ (615, 621.5, 624, 627.5, 629.5 nm) [20]. Their barycenters were found, respectively, at 490.71 nm (blue), 547.16 nm (green), 589.31 nm (orange) and 622.45 nm (red). As expected, for the UV–vis excitation of Tb^{3+} ions, green emission is the most intense.

The fluorescence decay curves for $^4G_{5/2}$ level of Lu_2O_3:Sm^{3+} and $^5D_4$ level of Lu_2O_3:Tb^{3+}, presented in Fig. 6, show complex decays with an exponential decay at longer times. For this reason it is more appropriate to calculate an average lifetime values for both samples

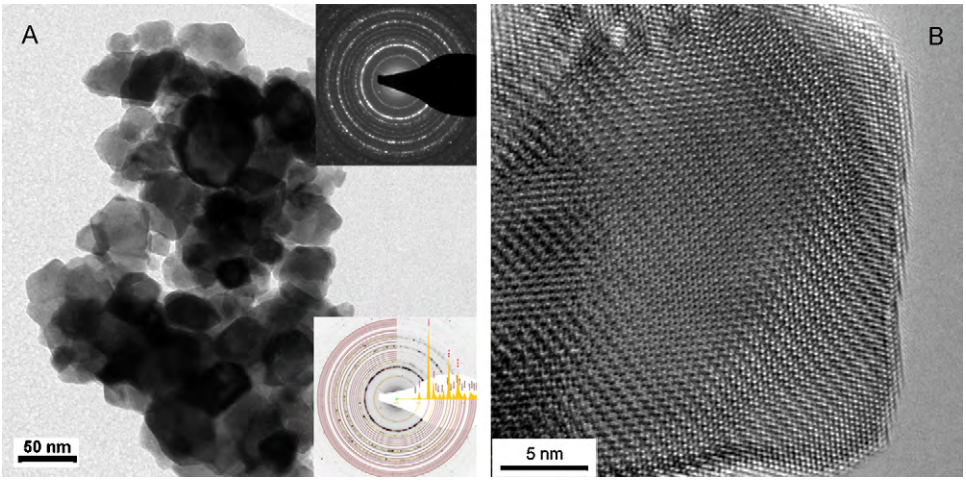

Fig. 4. Representative TEM image of one agglomerate in examined Lu_2O_3:Sm^{3+} sample (A) and HRTEM from one nanoparticle in the same agglomerate (B). Experimentally obtained ring electron diffraction pattern is presented in the upper right corner in part (A), and its match with XRD reflections is shown in the down right corner.

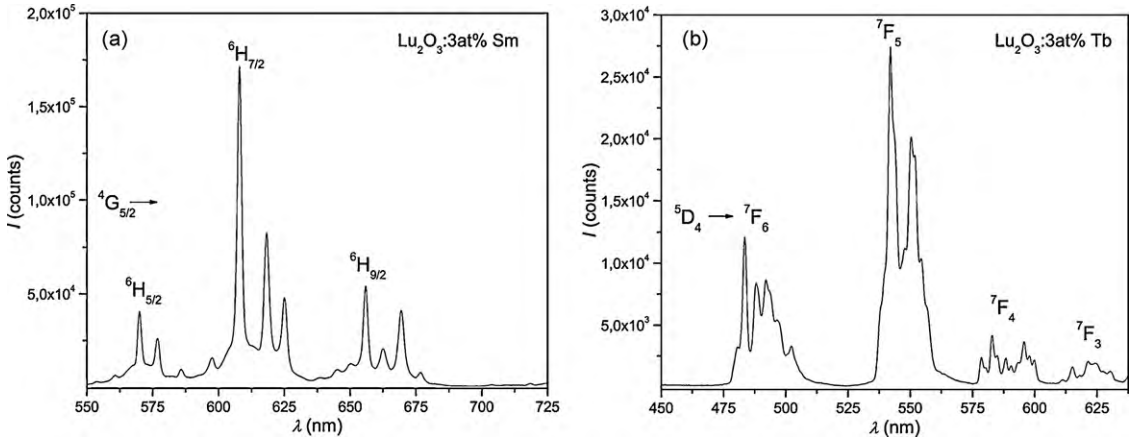

Fig. 5. Emission spectra of Lu_2O_3 samples: (a) reddish-orange of Sm^{3+} (λ_{exc} = 406 nm) and (b) pseudo-white emission of Tb^{3+} (λ_{exc} = 350 nm).

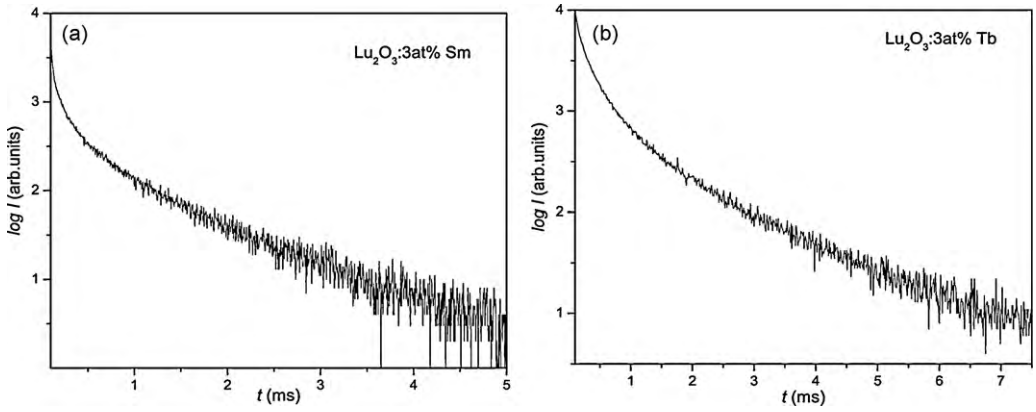

Fig. 6. The fluorescence decay curves of (a) $^4G_{5/2}$ for Sm^{3+} (λ_{exc} = 406 nm) and of (b) $^5D_4$ for Tb^{3+} (λ_{exc} = 350 nm) emitting levels in Lu_2O_3 samples.

using the following equation:

$$\tau_{avg} = \frac{\int_0^\infty tI(t)dt}{\int_0^\infty I(t)dt} \quad (1)$$

where $I(t)$ represents the luminescence intensity at time t corrected for the background, and the integrals are evaluated on a range $0 < t < t_m$ where $t_m \gg \tau_{avg}$ [21].

In this way average lifetime is calculated to be 0.8 and 0.6 ms for Sm^{3+} and Tb^{3+}-doped samples, respectively.

4. Conclusions

The synthesis based on the polymer complex solution method can be successfully used for the simple and low-cost production of pure-phase, C-type stable nanocrystalline lutetium oxide activated with Sm^{3+} and Tb^{3+} ions. The particles have sizes between 30 and 50 nm. EDX spectral analysis and mapping technique confirmed that samarium and terbium ions are fully and evenly integrated in the lutetium oxide solid solution. Optical properties were determined with the photoluminescence spectroscopy measurements in the energy and time domains. The samples exhibited characteristic luminescence emission of the dopant RE ions: with Sm^{3+} a reddish-orange emission is obtained, while doping with Tb^{3+} ions resulted in a combination of blue (mainly), green and red emission. Taking into account the simplicity of the synthesis process, the use of rather simple equipment, and low energy consumption, we found polymer complex solution synthesis appropriate for the production of good crystalline oxide phosphor materials such as Sm^{3+} and Tb^{3+} activated Lu_2O_3.

Acknowledgements

Authors from the Vinca Institute acknowledge the financial support of the Ministry of Science of the Republic of Serbia (Projects 142066). Dr. Krsmanović is also grateful to the NATO financial support (grant reference number CBP.EAP.RIG.983373).

References

[1] Z. Wang, W. Zhang, L. Lin, B. You, Y. Fu, M. Yin, Opt. Mater. 30 (2008) 1484–1488.
[2] Y. Shi, Q.W. Chen, J.L. Shi, Opt. Mater. 31 (2009) 729–733.
[3] D. Zhou, Y. Shi, P. Yun, J.J. Xie, J. Alloys Compd. 479 (2009) 870–874.
[4] P.S. Anil Kumar, J.J. Shrotri, S.D. Kulkarni, C.E. Deshpande, S.K. Date, Mater. Lett. 27 (1996) 293–296.
[5] L. Li, H.K. Yang, B.K. Moon, B.C. Choi, J.H. Jeong, K.H. Kim, Mater. Chem. Phys. 119 (2010) 471–477.
[6] N.A. Dulina, Y.V. Yermolayeva, A.V. Tolmachev, Z.P. Sergienko, O.M. Vovk, E.A. Vovk, N.A. Matveevskaya, P.V. Mateychenko, J. Eur. Ceram. Soc. 30 (2010) 1717–1724.
[7] Q. Chen, Y. Shi, L. An, S. Wang, J. Chen, J. Shi, J. Eur. Ceram. Soc. 27 (2007) 191–197.
[8] H. Wei, Z. Cleary, S. Park, K. Senevirathne, H. Eilers, J. Alloys Compd. (2010), doi:10.1016/j.jallcom.2010.03.220.
[9] A. García-Murillo, C. Le Luyer, C. Pedrini, J. Mugnier, J. Alloys Compd. 74–77 (2001) 323–324.
[10] D. Kulesza, J. Trojan-Piegza, E. Zych, Radiat. Meas. (2009), doi:10.1016/j.radmeas.2009.12.008.
[11] M. Galceran, M.C. Pujol, M. Aguiló, F. Díaz, Mater. Sci. Eng. B-Solid 146 (2008) 7–15.
[12] P.A. Lessing, Ceram. Bull. 68 (1989) 1002–1007.
[13] R.W. Cheary, A.A. Coelho, J. Appl. Crystallogr. 25 (1992) 109–121.
[14] L. Pauling, M.D. Shapell, Z. Kristallogr. 75 (1930) 128–142.
[15] R. Krsmanovic, P. Canton, A. Speghini, M. Bettinelli, S. Polizzi, Mater. Sci. Forum 453–454 (2004) 251–256.
[16] R. Krsmanović, S. Polizzi, P. Canton, Mater. Sci. Forum 494 (2005) 143–148.

[17] R. Krsmanović, O.I. Lebedev, A. Speghini, M. Bettinelli, S. Polizzi, G. Van Tendeloo, Nanotechnology 17 (2006) 2805–2812.
[18] P. Stadelmann, http://cime.epfl.ch/, http://cimewww.epfl.ch/people/stadelmann/jemsWebSite/jems.html (accessed: September 21st, 2004).
[19] Y. Li, Y. Chang, Y. Lin, Y. Chang, Y. Lin, J. Alloys Compd. 439 (2007) 367–375.
[20] B. Yan, H. Huang, J. Alloys Compd. 429 (2007) 338–342.
[21] E. Nakazawa, in: W.M. Yen, S. Shionoya, H. Yamamoto (Eds.), Phosphor Handbook, CRC Press, Boca Raton, 1999, pp. 11–20.